

# S3G-ARM: Highly Compressive Visual Self-localization from Sequential Semantic Scene Graph Using Absolute and Relative Measurements

Yoshida Mitsuki

Yamamoto Ryogo

Tanaka Kanji

**Abstract**—In this paper, we address the problem of image sequence-based self-localization (ISS) from a new highly compressive scene representation called sequential semantic scene graph (S3G). Recent developments in deep graph convolutional neural networks (GCNs) have enabled a highly compressive visual place classifier (VPC) that can use a scene graph as the input modality. However, in such a highly compressive application, the amount of information lost in the image-to-graph mapping is significant and can damage the classification performance. To address this issue, we propose a pair of similarity-preserving mappings, image-to-nodes and image-to-edges, such that the nodes and edges act as absolute and relative features, respectively, that complement each other. Moreover, the proposed GCN-VPC is applied to a new task of viewpoint planning (VP) of the query image sequence, which contributes to further improvement in the VPC performance. Experiments using the public NCLT dataset validated the effectiveness of the proposed method.

## I. INTRODUCTION

Image sequence-based self-localization (ISS) has received considerable attention as a highly compressive and discriminative approach to long-term visual place recognition (VPR) across domains (e.g., weather, time of day, and season). Given a long-term image sequence  $I_1^{map}, \dots, I_T^{map}$  covering the robot workspace in a past domain (“map”), the ISS aims to determine the most matched sub-sequence for a short-term query sequence  $I_{t_1}^{query}, \dots, I_{t_N}^{query}$  ( $|t_N - t_1| \ll T$ ) in a new unseen domain [1]. An advantage of this ISS approach is a good balance between the discriminative power and compactness. Even in highly compressive applications (e.g., 4-bit image descriptor [2]) where typical single-view self-localization approaches suffer, the ISS approach may maintain high performance owing to the multi-view information fusion. Moreover, such a map can be flexibly reorganized into a local map  $I_a, \dots, I_b$  with arbitrary start  $a$  and goal  $b$  viewpoints ( $|b - a| < T$ ), which enables an efficient reuse of storage in applications such as multi-robot multi-session knowledge sharing [3].

In this study, we explore the ISS problem from a novel perspective of sequential semantic scene graph (S3G), as shown in Fig. 1. The motivation for this approach is threefold. First, semantic scene graph (S2G)  $x^G = \langle x^N, x^E \rangle$ , a graph whose nodes  $x^N$  represent semantic regions (e.g., object regions) and edges  $x^E$  represent relationship between nodes, is one of most compact scene descriptors in computer vision [4]. Second, recently-developed deep graph convolutional neural networks

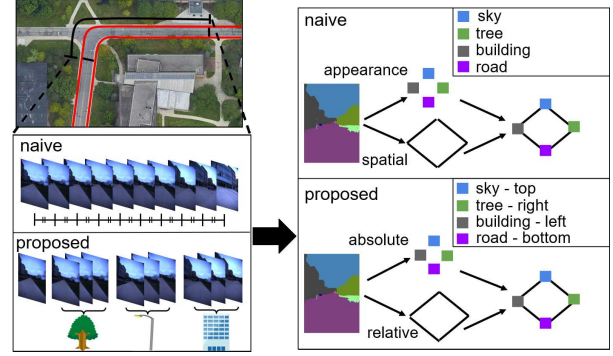


Fig. 1. Visual place recognition (VPR) from a novel highly compressive sequential semantic scene graph (S3G) is considered. To address the information lost in dimension reduction, the appearance/spatial image information is mapped to two different features, absolute (node) and relative (edge) features, which complement each other. Additionally, a new task of viewpoint planning (VP) of the query S3G is enabled by the trained VPR, to further improve the VPR performance.

(GCNs) can serve as a powerful visual-place-classifier (VPC)  $y = f_{VPC}(x)$  that takes a scene graph  $x$  as query and predicts the place class  $y$  [5]. Third, such a well-trained VPC is noted to provide useful information for viewpoint planning (VP) of the query sequence  $I_{t_1}^{query}, \dots, I_{t_N}^{query}$ , to further improve the VPR performance. The remaining issue is how to design an effective similarity-preserving mapping  $x^G = f_{IG}(I)$  from an input image  $I$  to a scene graph  $x^G$ .

Here, we propose to exploit a pair of similarity-preserving-mappings, image-to-nodes  $x^N = f_{IN}(I)$  and image-to-edges  $x^E = f_{IE}(I)$ , which provide two forms (i.e., nodes  $x^N$  and edges  $x^E$ ) of appearance/spatial image features. In earlier approaches, the appearance and spatial image features are separately mapped to nodes and edges, respectively (i.e., appearance-to-nodes, and spatial-to-edges) [6]. However, in our highly compressive application, the amount of information lost in the dimension-reduction is significant that recognition errors can be frequently yielded in a mapping. In the proposed approach, the nodes  $x^N$  and edges  $x^E$  act as *absolute* (e.g., size and brightness) and *relative* (e.g., larger and brighter) that complement each other, to further improve the overall VPR performance.

Our contributions were as follows. (1) We presented a highly compressive S3G-based VPR approach. S3G is an extension of the ISS framework toward the application of an S2G. Moreover, we addressed the VP to control the viewpoints of the S3G to further improve the overall VPR performance. (2) We proposed a pair of similarity-preserving mappings, image-to-nodes and image-to-edges,

Our work has been supported in part by JSPS KAKENHI Grant-in-Aid for Scientific Research (C) 17K00361 and 20K12008.

The authors are with Graduate School of Engineering, University of Fukui, Japan. [tnkknj@u-fukui.ac.jp](mailto:tnkknj@u-fukui.ac.jp)

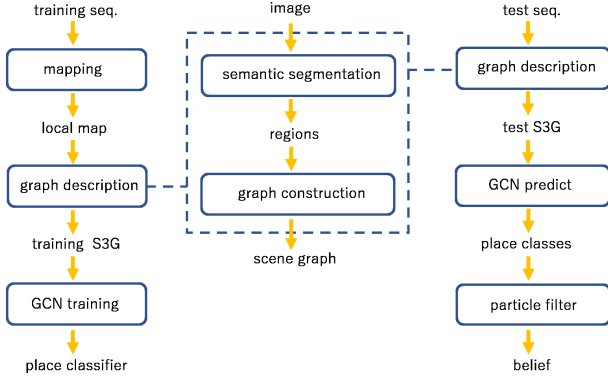


Fig. 2. Algorithm pipeline. In the training/test stage, input images are converted to an S3G and then fed to the GCN training/test module. In the test stage, the prediction results at each viewpoint are further integrated by a particle filter, to obtain the final estimate.

such that the absolute features (i.e., nodes) and relative features (i.e., edges) complement each other. (3) We implemented a prototype system of the proposed framework for simultaneous VPR and VP, and validated the effectiveness of the proposed method through experimental comparisons and ablation studies using the public NCLT dataset [7].

## II. APPROACH

Figure 2 illustrates the architecture of the proposed system. The system includes the (offline) training module and (on-line) test module. In addition, a scene graph descriptor submodule is employed by both the training and test modules. These modules are detailed in the following subsections.

### A. Edge: Relative Feature

There exist several possible approaches to constructing graph edges from an input query/map image sequence (Fig. 3). The first approach is to view each image frame in the sequence as a graph node and connect neighboring image nodes by edges [5] (Fig. 3a). The second approach is to apply pre-defined partitioning, such as grid-based partitioning, to obtain spatio-temporal node regions (Fig. 3b). The third approach is to employ semantic video segmentation techniques to segment an input image sequence (video clip) into spatio-temporal region nodes (Fig. 3c). The fourth approach employs image segmentation techniques to segment images into image region nodes (Fig. 3d).

In this study, we adopted an image scene graph with image region nodes (i.e., the fourth approach) for the following reasons. The first approach is simple and effective. Indeed, in our earlier system on GCN-based VPR [5], each image frame is partitioned into predefined regions (e.g., “center,” “left,” “right”). However, such a graph structure does not reflect the scene layout, i.e., provides no information. In experiments, we used this approach as the baseline method. The second and third approaches are prohibitive in our application; hence, in these approaches, the start/goal endpoints of individual sequences must be defined during the training stage, and cannot be controlled on the fly during

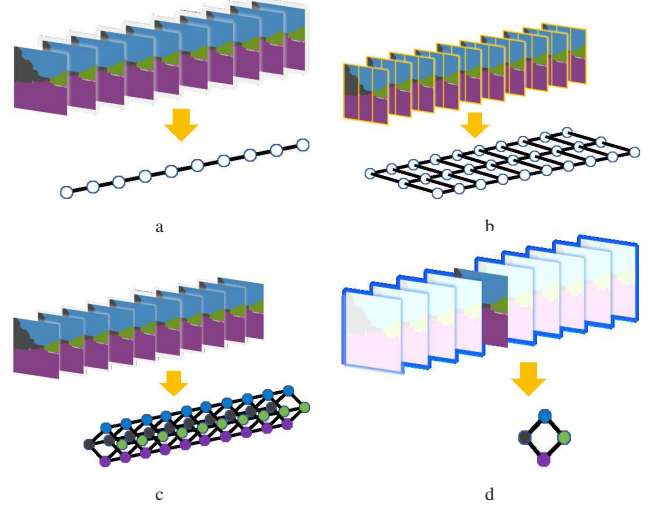


Fig. 3. Different representations of a scene graph. (a) Single-view image graph. (b) Multi-view grid-based segmentation. (c) Multi-view semantic video clip segmentation. (d) Single-view semantic image segmentation.

the testing stage. In contrast, the fourth approach is flexible and informative. Unlike the second and third approaches, it allows a map-user robot to flexibly control the endpoints on the fly during the testing stage. Moreover, unlike in the first approach, the graph edges reflect the scene layout, thus yielding informative scene graphs.

The procedure for graph construction is as follows. First, semantic labels are assigned to pixels using DeepLab v3+ [8], pretrained on Cityscapes dataset. Then, regions smaller than 100 pixels are regarded as noise and removed. Subsequently, connected regions with the same semantic labels are identified using a flood-fill algorithm [9], and each is assigned a unique region ID. Next, each region is connected to each of its neighboring regions by an edge. Finally, an image scene graph with image region nodes is obtained.

### B. Node: Absolute Feature

Image region descriptors (i.e., node descriptor in our case) have been intensively studied. Existing descriptors can be generally categorized into two groups: local features [10] and global features [11]. Most are in the form of high-dimensional feature vectors [11], or an unordered collection of vector quantized features called “bag-of-words” [12]. However, their space costs increase in proportion to the number and dimensionality of the original feature vectors, and typically require a hundreds or thousands of bytes per scene. This is expensive in our highly compressive application.

In the field of image retrieval, semantic labels (e.g., object category IDs) have been used as extremely compact descriptors that can be used for indexing and retrieving images [13].

A key difference of our robotics application from these image retrieval applications is that in robotics, the semantics of surrounding objects and their spatial information such as bearing (“B”) and range (“R”) play important roles in VPR. Indeed, in the field of robotic SLAM, there have been

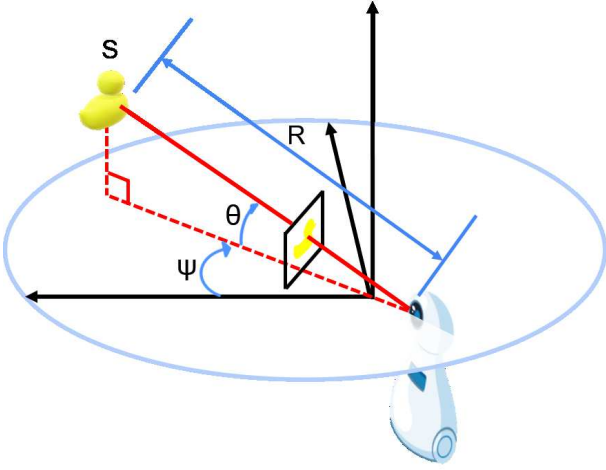


Fig. 4. Bearing-range-semantic (BRS) measurement model. The bearing, range, and semantics are observed in an image, as the location, size, and semantic label, respectively, of an object region. Then, the three-dimensional B-R-S space is quantized to obtain a compact 189-dim 1-hot vector (i.e., an 8-bit descriptor).

special interest groups of researches focusing on different types of spatial information, namely, range-bearing SLAM [14], range-only SLAM [15], and bearing-only SLAM [16].

Based on the aforementioned consideration, our VPR task was formulated as a bearing-range-semantic (BRS) measurements-based VPR (Fig. 4).

Specifically, in our approach, the semantic labels output by a semantic segmentation network [17] were re-categorized into seven different semantic category IDs: “sky,” “tree,” “building,” “pole,” “road,” “traffic sign,” and “the others” which respectively correspond to the labels {“sky”}, {“vegetation”}, {“building”}, {“pole”}, {“road,” “sidewalk”}, {“traffic-light,” “traffic-sign”}, and {“person,” “rider,” “car,” “truck,” “bus,” “train,” “motorcycle,” “bicycle,” “wall,” “fence,” “terrain”} in the original label space. The location of the region center was quantized by a  $3 \times 3$  regular grid into nine “bearing” category IDs. The region size was quantized into three “range” category IDs: “short distance (larger than 150 K pixels),” “medium distance (50 K-150 K pixels),” and “long distance (smaller than 50 K)” for  $616 \times 808$  image. Finally, these semantic, bearing and range category IDs are combined to obtain a 189-dim 1-hot vector as the node descriptor.

At first glance, the use of edges as additional features might look unnecessary, because both the appearance and spatial features are already included in the node features. However, its objectives are quite different. In other words, the edge descriptor is suitable for describing the relative feature (e.g., position-relationship) rather than the absolute feature (e.g., position). The nodes and edges can act as error detection codes [18] that complement each other. Figure 5 illustrates an example showing how the edge features help to discriminate a nearly duplicate S2G pair, which the node descriptor alone could not discriminate.

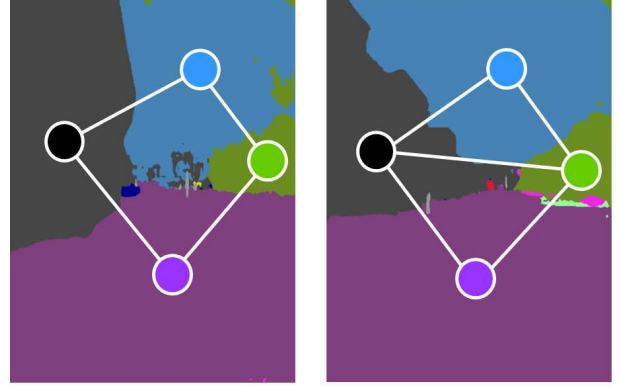


Fig. 5. Importance of edges. In highly compressive applications, a naive strategy of using only absolute features (i.e., nodes) suffer from information loss during dimension reduction. To address this issue, we exploit the edges as relative features that complement the absolute features.

### C. Region Merging

Most existing techniques for semantic segmentation trade domain-invariance for accuracy. Their objective function and performance index place the highest priority on pixel-level precision/recall accuracy, i.e., detecting semantically coherent regions as accurately as possible. Hence, their graph topology is often affected by the other factors, such as viewpoint drift and occlusions. This is problematic for our VPR application as the graph topology is a primary cue that dominates the GCN performance.

To address this issue, we adopted a region merging technique, inspired by a recent work in [19]. Specifically, we remove small regions whose areas are smaller than 1,000 pixels (for  $616 \times 808$  image). We noted this simple technique to be very effective in improving VPR performance, as illustrated through ablation studies in the experimental section (III).

### D. Self-localization from S2G

Self-localization from S2G is directly addressed by GCN-based VPC. It takes a single-view image and predicts the place class. The GCN is the most popular approach to graph neural networks. It has been successfully used in various applications, including web-scale recommender systems [20], and chemical reactivity [21]. In our recent study [5], a GCN is trained as an image-sequence classifier (i.e., Fig. 3a) and achieved the state-of-the-art VPR performance.

For the definition of place classes, we follow the grid-based partitioning in [22]. In the experimental environment, this yields  $10 \times 10$  grid cells and 100 place classes in total.

In this study, we trained a GCN using the S2Gs as the training data. The graph convolution operation takes node  $v_i$  in the graph and processes it in the following manner. First, it receives messages from nodes connected by the edge. The collected messages are then summed via the SUM function. The result is passed through a single-layer fully connected neural network followed by a nonlinear transformation for conversion into a new feature vector. In this study, we used



the rectified linear unit (ReLU) operation as the nonlinear transformation, which is expressed as follows:

$$\mathbf{h}_i^{new} = \text{ReLU} \left( \mathbf{W} \left( \sum_{u \in N(v_i) \cup v_i} \mathbf{h}_u \right) \right). \quad (1)$$

Here,  $\mathbf{W}$  represents an  $R^{D \times F}$  weight matrix, and  $D$  and  $F$  represent the numbers of dimensions of the node feature vector before and after the linear transformation, respectively. The foregoing process can be generalized to the processing of node features in each  $l$ -th GCN layer. The process was applied to all the nodes in the graph in each iteration, yielding a new graph that had the same shape as the original graph but updated node features. The iterative process was repeated  $L$  times, where  $L$  represents the ID of the last GCN layer. After the graph node information obtained in this manner were averaged, the probability value vector of the prediction for the graph was obtained by applying the fully connected layer and the softmax function. For the probability value vector of the output  $p$ , the operation is expressed as follows:

$$\mathbf{p} = \text{Softmax} \left( FC \left( \frac{1}{|V|} \sum_{u \in V} \mathbf{h}_u^L \right) \right). \quad (2)$$

where  $h_u$  represents a feature of node  $u$  after it passes through the last GCN layer. For implementation, we used the deep graph library [23] on the Pytorch backend.

#### E. Self-localization from S3G

The ISS system aims to estimate the robot location from a sequence of S2Gs (i.e., S3G). It consists of two modules: information fusion and viewpoint planning.

The information fusion module employs a particle filter (PF) to incorporate the history of perceptual-action measurements  $I_{t_1}^{query}, \dots, I_{t_n}^{query}$  at each viewpoint  $t_n$  of the query image sequence into the current belief of the robot location, as in [24]. An action corresponds to a forward movement along the viewpoint trajectory, and a perception corresponds to a class-specific probability density vector (PDV) output by the GCN. In the measurement update, each particle is categorized into a place class, and its weight is updated by incorporating the PDV value of the class to which the particle's hypothesized location belongs.

The viewpoint planning (VP) is formulated as a reinforcement-learning (RL) problem, in which a learning agent interacts with a stochastic environment. The interaction is modeled as a discrete-time discounted Markov decision process (MDP). A discounted MDP is a quintuple  $(S, A, P, R, \gamma)$ , where  $S$  and  $A$  are the set of states and actions, respectively,  $P$  denotes the state transition distribution,  $R$  denotes the reward function, and  $\gamma \in (0, 1)$  denotes a discount factor ( $\gamma = 0.9$ ). We denoted  $P(\cdot|s, a)$  and  $r(s, a)$  as the probability distribution over the next state and the immediate reward of performing action  $a$  for state  $s$ , respectively. State  $s$  is defined as the belief in the form of class-specific reciprocal rank vector, as in [25]. Action  $a$  is defined as a forward movement along the route. In the experiments, the action candidate set was  $A = \{1, 2, \dots, 10\}$  (m). A training/test

TABLE I  
PERFORMANCE RESULTS.

		w/ region merging		w/o region merging	
		S	BRS	S	BRS
VPR	GCN	11.7	18.9	12.0	19.1
	KNN	5.8	15.6	6.3	12.9
	NBNN	1.3	3.4	1.4	3.5
VPR+VP	GCN	-	30.6	-	-
	KNN	-	-	-	-
	NBNN	-	-	-	-

episode was a 10 sequential action. We addressed the issue of the curse of dimensionality in RL by employing the recently developed nearest neighbor approximation of Q-learning (NNQL) [26] with  $k = 4$ . The immediate reward was provided at the final viewpoint of each train episode, as the reciprocal rank value of the ground truth viewpoint. The learning rate was set to  $\alpha = 0.1$ .

### III. EXPERIMENTS

The proposed method was evaluated in a cross-season self-localization scenario. The goal of the evaluation was to validate whether the GCN-based VPR method could boost the performance in both passive VPR and active VPR (i.e., VPR-VP) scenario.

The public NCLT dataset [7] was used in the experiments (Fig. 6). The NCLT dataset is a dataset for long-term autonomy obtained using a Segway vehicle at the University of Michigan North Campus. While the vehicle travels seamlessly indoors and outdoors, the vehicle encountered various geometric changes (e.g., object placement changes, pedestrians, car parking/stopping) and photometric changes (e.g., lighting conditions, shadows, and occlusions). In particular, we assumed challenging cross-season self-localization scenarios, in which the self-localization system is trained and tested in different seasons. To this end, four pairings of (training, test) seasons were created from four different seasons' datasets "2012/1/22 (WI)," "2012/3/31 (SP)," "2012/8/4 (SU)," and "2012/11/17 (AU)": (WI, SP), (SP, SU), (SU, AU), and (AU, WI). Additionally, an extra season "2012/5/11 (EX)" was used to train VPR. That is, VPR was trained only once in the season EX prior to the self-localization tasks, and then the learned VPR parameters

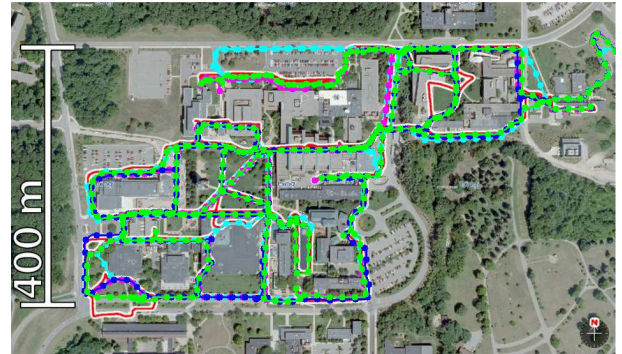


Fig. 6. Experimental environments. The trajectories of the four datasets, "2012/1/22," "2012/3/31," "2012/8/4," and "2012/11/17," used in our experiments are visualized in green, purple, blue, and light-blue curves, respectively.



Fig. 7. S2G examples. Top: The input image. Bottom: S2G overlaid on the semantic label image.

were commonly used for training and testing the VPR-VPR system.

Three different VPR methods, GCN, naive Bayes nearest neighbor (NBNN), and k-nearest neighbor (kNN) were evaluated. All took an image sequence represented as an S3G, as input. The GCN is the proposed method described in Section II. Because no prior study exists on the highly compressive S3G applications, our investigation mainly focused on developing and evaluating as various possible ablations of this method as possible. NBNN and kNN methods are based on measuring dissimilarities in the node feature set between a query-map pair of interest. NBNN [27] is a best known method to measure dissimilarities between such a feature set pair, and has shown high performance in our earlier studies (e.g., [28]). In that, the L2 distance from the nearest-neighbor map feature to each query feature is computed, and then it is averaged over all the query features, which yields the NBNN dissimilarity value. kNN is a traditional non-parametric classification method based on the nearest-neighbor training sample in the feature space, in which the class labels most often assigned to the training samples of the kNN (i.e., minimum L2 norm) are returned as classification results. In that, an image is described by a 189-dim histogram vector by aggregating all the node features that belong to the image.

VPR performance was evaluated in terms of top-1 accuracy. The evaluation procedure was as follows. First, VPR performance at all viewpoints of the query sequence, and not just the final viewpoint, were computed. Then, top-1 accuracy at each viewpoint was computed from the latest PF output based on whether the class with highest belief value matches the ground-truth.

Figure 7 demonstrates scene graphs obtained using the proposed scene graph construction procedure. Notably, the domain-invariant parts (e.g., buildings and roads) of the input scenes tended to be selected as the landmark regions.

An ablation study was conducted to observe the effects of individual components, including the relative edge feature (Section II-A) and region merging technique (Section II-C). Table I lists the results of all combinations of the proposed and baseline methods. Notably, the proposed method yielded

a superior performance compared to all other methods considered here. The technique of region merging (Section II-C) contributed to reduce the number of nodes while retaining the VPR performance. The number of nodes was reduced from 19.8 to 7.2 per S2G on average, which results in the reduction of computation time for VPR from 0.82 ms to 0.16 ms. Particularly, the use of edge feature and the NBV module often significantly boosted the VPR performance.

Finally, we investigated space costs. The number of nodes per S2G was 7.2 on average. The node descriptor consumed 8-bit per node. The space cost for nodes and edges were 57.8-bit and 12.5-bit per S2G, respectively, on average. Notably, the current descriptors were not compressed, i.e., they may be further compressed.

#### IV. CONCLUSIONS

In this study, a novel highly compressive VPR framework for ISS was proposed using S3Gs. For such a highly compressive application, the amount of information lost in the dimension reduction is significant and can damage the VPR performance. To address this issue, we proposed the exploitation of a pair of similarity-preserving mappings, image-to-nodes and image-to-edges, such that the nodes and edges complement each other. Moreover, the S3G framework was applied to the VPR and VP task to control the viewpoints of an S3G to further improve the performance. Experiments using the public NCLT dataset with performance comparisons and ablation studies validated the effectiveness of the proposed method.

#### REFERENCES

- [1] M. J. Milford and G. F. Wyeth, “Seqslam: Visual route-based navigation for sunny summer days and stormy winter nights,” in *2012 IEEE International Conference on Robotics and Automation*, 2012, pp. 1643–1649.
- [2] F. Yan, O. Vysotska, and C. Stachniss, “Global localization on openstreetmap using 4-bit semantic descriptors,” in *2019 European Conference on Mobile Robots (ECMR)*. IEEE, 2019, pp. 1–7.
- [3] M. T. Lazaro, L. M. Paz, P. Pinies, J. A. Castellanos, and G. Grisetti, “Multi-robot slam using condensed measurements,” in *2013 IEEE/RSJ International Conference on Intelligent Robots and Systems*. IEEE, 2013, pp. 1069–1076.
- [4] J. Yang, J. Lu, S. Lee, D. Batra, and D. Parikh, “Graph r-cnn for scene graph generation,” in *Proceedings of the European conference on computer vision (ECCV)*, 2018, pp. 670–685.
- [5] K. Takeda and K. Tanaka, “Dark reciprocal-rank: Teacher-to-student knowledge transfer from self-localization model to graph-convolutional neural network,” in *2021 International Conference on Robotics and Automation (ICRA)*, 2021, pp. 4348–4355.
- [6] Y. Zhu, Y. Ma, L. Chen, C. Liu, M. Ye, and L. Li, “Gosmatch: Graph-of-semantics matching for detecting loop closures in 3d lidar data,” in *2020 IEEE/RSJ International Conference on Intelligent Robots and Systems (IROS)*. IEEE, 2020, pp. 5151–5157.
- [7] N. Carlevaris-Bianco, A. K. Ushani, and R. M. Eustice, “University of michigan north campus long-term vision and lidar dataset,” *The International Journal of Robotics Research*, vol. 35, no. 9, pp. 1023–1035, 2016.
- [8] L.-C. Chen, Y. Zhu, G. Papandreou, F. Schroff, and H. Adam, “Encoder-decoder with atrous separable convolution for semantic image segmentation,” in *Proceedings of the European conference on computer vision (ECCV)*, 2018, pp. 801–818.
- [9] Y. He, T. Hu, and D. Zeng, “Scan-flood fill (scaff): An efficient automatic precise region filling algorithm for complicated regions,” in *Proceedings of the IEEE/CVF Conference on Computer Vision and Pattern Recognition Workshops*, 2019, pp. 0–0.

- [10] A. Oliva and A. Torralba, "Modeling the shape of the scene: A holistic representation of the spatial envelope," *International journal of computer vision*, vol. 42, no. 3, pp. 145–175, 2001.
- [11] D. G. Lowe, "Distinctive image features from scale-invariant keypoints," *International journal of computer vision*, vol. 60, no. 2, pp. 91–110, 2004.
- [12] J. Sivic and A. Zisserman, "Video google: A text retrieval approach to object matching in videos," in *null*. IEEE, 2003, p. 1470.
- [13] P. Hiremath and J. Pujari, "Content based image retrieval using color, texture and shape features," in *15th International Conference on Advanced Computing and Communications (ADCOM 2007)*. IEEE, 2007, pp. 780–784.
- [14] M. Ramezani, G. Tinchev, E. Iuganov, and M. Fallon, "Online lidar-slam for legged robots with robust registration and deep-learned loop closure," in *2020 IEEE International Conference on Robotics and Automation (ICRA)*. IEEE, 2020, pp. 4158–4164.
- [15] Y. Song, M. Guan, W. P. Tay, C. L. Law, and C. Wen, "Uwb/lidar fusion for cooperative range-only slam," in *2019 international conference on robotics and automation (ICRA)*. IEEE, 2019, pp. 6568–6574.
- [16] E. Bj, T. A. Johansen, *et al.*, "Redesign and analysis of globally asymptotically stable bearing only slam," in *2017 20th International Conference on Information Fusion (Fusion)*. IEEE, 2017, pp. 1–8.
- [17] O. Ronneberger, P. Fischer, and T. Brox, "U-net: Convolutional networks for biomedical image segmentation. arxiv 2015," *arXiv preprint arXiv:1505.04597*, 2019.
- [18] A. D. Córcoles, E. Magesan, S. J. Srinivasan, A. W. Cross, M. Steffen, J. M. Gambetta, and J. M. Chow, "Demonstration of a quantum error detection code using a square lattice of four superconducting qubits," *Nature communications*, vol. 6, no. 1, pp. 1–10, 2015.
- [19] B. Matejek, D. Haehn, H. Zhu, D. Wei, T. Parag, and H. Pfister, "Biologically-constrained graphs for global connectomics reconstruction," in *Proceedings of the IEEE/CVF Conference on Computer Vision and Pattern Recognition*, 2019, pp. 2089–2098.
- [20] R. Ying, R. He, K. Chen, P. Eksombatchai, W. L. Hamilton, and J. Leskovec, "Graph convolutional neural networks for web-scale recommender systems," in *Proceedings of the 24th ACM SIGKDD Int. Conf. Knowledge Discovery & Data Mining*, 2018, pp. 974–983.
- [21] C. W. Coley, W. Jin, L. Rogers, T. F. Jamison, T. S. Jaakkola, W. H. Green, R. Barzilay, and K. F. Jensen, "A graph-convolutional neural network model for the prediction of chemical reactivity," *Chemical science*, vol. 10, no. 2, pp. 370–377, 2019.
- [22] G. Kim, B. Park, and A. Kim, "1-day learning, 1-year localization: Long-term lidar localization using scan context image," *IEEE Robotics and Automation Letters*, vol. 4, no. 2, pp. 1948–1955, 2019.
- [23] M. Wang, L. Yu, D. Zheng, Q. Gan, Y. Gai, Z. Ye, M. Li, J. Zhou, Q. Huang, C. Ma, Z. Huang, Q. Guo, H. Zhang, H. Lin, J. Zhao, J. Li, A. J. Smola, and Z. Zhang, "Deep graph library: Towards efficient and scalable deep learning on graphs," *ICLR Workshop on Representation Learning on Graphs and Manifolds*, 2019.
- [24] F. Dellaert, D. Fox, W. Burgard, and S. Thrun, "Monte carlo localization for mobile robots," in *1999 International Conference on Robotics and Automation (ICRA)*, vol. 2, 1999, pp. 1322–1328.
- [25] K. Tanaka, "Active map-matching: Teacher-to-student knowledge transfer from visual-place-recognition model to next-best-view planner for active cross-domain self-localization," in *2021 IEEE International Conference on Computational Intelligence and Virtual Environments for Measurement Systems and Applications (CIVEMSA)*. IEEE, 2021, pp. 1–6.
- [26] D. Shah and Q. Xie, "Q-learning with nearest neighbors," *arXiv preprint arXiv:1802.03900*, 2018.
- [27] T. Tommasi and B. Caputo, "Frustratingly easy nbnn domain adaptation," in *Proceedings of the IEEE International Conference on Computer Vision*, 2013, pp. 897–904.
- [28] K. Tanaka, "Cross-season place recognition using nbnn scene descriptor," in *2015 IEEE/RSJ International Conference on Intelligent Robots and Systems (IROS)*. IEEE, 2015, pp. 729–735.